ACADÉMIE
DES SCIENCES
INSTITUT DE FRANCE

Comptes Rendus
Physique

François Pétrélis

Experimental dynamos: from models to applications to the geodynamo

Volume 25, Special Issue S3 (2024), p. 611-627

Online since: 3 December 2024

Part of Special Issue: Geophysical and astrophysical fluid dynamics in the laboratory
Guest editors: Stephan Fauve (Laboratoire de Physique de l'ENS, CNRS, PSL Research University, Sorbonne Université, Université Paris Cité, Paris, France) and Michael Le Bars (CNRS, Aix Marseille Univ, Centrale Marseille, IRPHE, Marseille, France)

https://doi.org/10.5802/crphys.205

The Comptes Rendus. Physique *are a member of the Mersenne Center for open scientific publishing*
www.centre-mersenne.org — e-ISSN : 1878-1535

ACADÉMIE DES SCIENCES
INSTITUT DE FRANCE

Comptes Rendus. Physique
2024, Vol. 25, Special issue S3, p. 611-627
https://doi.org/10.5802/crphys.205

Research article / *Article de recherche*

Geophysical and astrophysical fluid dynamics in the laboratory / *Dynamique des fluides géophysiques et astrophysiques au laboratoire*

Experimental dynamos: from models to applications to the geodynamo

Dynamos expérimentales : des modèles aux applications à la géodynamo

François Pétrélis [a]

[a] LPENS, CNRS, ENS Paris, PSL University, Sorbonne Université, Université de Paris, F-75005, Paris, France

Abstract. Larmor proposed in 1919 an explanation for the origin of the Sun's magnetic field. This phenomenon, known as the dynamo effect, is considered to be responsible for most of the magnetic fields of astrophysical objects, including that of the Earth. It took over 80 years after Larmor's explanation for the first laboratory experiments to demonstrate the dynamo instability. After a brief introduction to the three experiments that have managed to observe this effect, I will describe what they have taught us about the possible regimes of dynamos of planets and stars, especially regarding the geodynamo.

Résumé. Larmor a proposé en 1919 une explication pour l'origine du champ magnétique du soleil. Cette instabilité dite effet dynamo est considérée comme responsable de la plupart des champs magnétiques des objets astrophysiques dont celui de la Terre. Il a fallu plus de 80 ans après l'explication par Larmor pour que les premières expériences de laboratoire mettent en évidence l'instabilité dynamo. Après une brève présentation des trois expériences qui ont réussi à observer cet effet, je décris ce qu'elles nous ont appris sur les régimes possibles des dynamos des planètes et des étoiles et notamment sur la géodynamo.

Keywords. Magnetohydrodynamics, dynamo instability, reversals of the Earth's magnetic field.

Mots-clés. Magnétohydrodynamique, instabilité dynamo, inversions du champ magnétique terrestre.

Manuscript received 9 April 2024, revised 30 July 2024, accepted 4 September 2024.

1. Introduction

The Earth and the Sun both generate a magnetic field that can easily be measured at their surface. This is also true for most planets and stars.

It was Larmor in 1919 who first proposed that the origin of the Sun's magnetic field is a dynamo instability: in an electrically conductive fluid, part of the kinetic energy of the flow is converted into magnetic energy [1]. A similar effect was known for solid dynamos, consisting of electrical windings and magnetic structures. Modern investigations of solid dynamos are discussed in [2–4].

Planetary interiors, containing electrically conductive liquid zones, have led to the dynamo instability being commonly accepted as the mechanism generating the magnetic fields of planets, including that of Earth.

For a long time after Larmor's initial publication, most results obtained were theoretical and numerical in the more recent period, for reviews see [5,6].

It took more than 80 years before the first laboratory observations of the dynamo effect in conductive fluids were achieved. To date, there are three experiments that have demonstrated this effect. A dynamo based on a helical flow in Riga, Latvia [7], a dynamo based on an array of helical flows in Karlsruhe, Germany [8], and a dynamo based on a swirling flow between two counter-rotating coaxial disks in Cadarache, France [9]. We note that there had been other attempts that remained unsuccessful to observe the dynamo instability even though they were able to measure induction mechanisms [10–12].

In this article, we will briefly review what the three successful experiments have taught us, an in particular how they have contributed to the understanding of the magnetic fields of astrophysical objects. A more extensive review on the generation of magnetic field by experimental dynamos can be found in [13]. Here the focus is made on the dynamical features of the magnetic field generated in the experimental dynamos and we show that their understanding provides an explanation for the dynamical regimes of natural dynamos and in particular for the random reversals of the geodynamo.

2. Description of the three fluid dynamo experiments

2.1. *Generic features of experimental dynamos*

The three experiments share common properties. The electrically conductive fluid is liquid sodium maintained above its melting temperature, nearly 98°C.

As we will see in the description of each experiment, the order of magnitude of the experiments' size is the meter, and setting the fluid in motion requires mechanical powers greater than one hundred kilowatts.

These properties are actually required by the nature of the instability. As they are also responsible for the difficulty to perform such experiments, it is interesting to understand their origin. Let us consider an experiment with a liquid of electrical conductivity σ, density ρ, kinematic viscosity ν and magnetic permeability the one of vacuum μ_0. The fluid flows at characteristic speed V with a typical size L.

The dynamo instability takes place when the source of growth of the magnetic field overcomes the dissipative terms. More precisely, in the induction equation

$$\frac{\partial \mathbf{B}}{\partial t} = \nabla \times (\mathbf{v} \times \mathbf{B}) + \frac{1}{\mu_0 \sigma} \nabla^2 \mathbf{B}, \tag{1}$$

when the ratio of the first to the second term of the right hand side is large enough. Estimating these terms, we define their ratio by the magnetic Reynolds number $R_m = \mu_0 \sigma V L$. The dynamo instability onset is associated to a critical value of R_m which is of order $10 - 100$ in the flows used in the experiments.

A second dimensionless number controls the properties of such systems. It is convenient to use the magnetic Prandtl number $P_m = \mu_0 \sigma \nu$. Values of P_m are smaller than 10^{-5} for liquid metals. This is actually constrained by the physics of liquid metals. Indeed, ν measures the microscopic transport of momentum and $(\mu_0 \sigma)^{-1}$ the one of electricity. They take quite different values in liquid metals as electricity is carried by electrons and impulsion by the nucleus of the atoms. These quantities can be calculated using Drude's law for the electrical conductivity and standard estimates of the viscosity of fluids. This provides orders of magnitude built upon

microscopic quantities. Ultimately, we obtain an estimate of the magnetic Prandtl number, that can be written in a compact form as

$$P_m = \alpha^2 \sqrt{\frac{m_e}{m_p}}, \tag{2}$$

where $\alpha = q^2/(\hbar c) \simeq 137^{-1}$ is the fine structure constant and m_e and m_p are the masses of an electron and a proton. This leads to $P_m \simeq 10^{-6}$ which order of magnitude compares well with the values for liquid metals in the vicinity of their melting temperature. The small value of the magnetic Prandtl number thus results from the smallness of the mass ratio between electrons and protons, and from the smallness of the fine structure constant.

A consequence of this property is that, at onset of the dynamo instability, the kinematic Reynolds number $Re = VL/\nu = R_m/P_m$ reaches very large values, superior to 10^6. Dynamo unstable flow are thus highly turbulent.

We can then estimate the power P needed to drive the turbulent which is, in order of magnitude, $P = \rho R_m^3/(L\mu_0^3\sigma^3)$. This leads to an estimate of $100kW$ for a 1 meter flow of liquid sodium at R_m of order fifty [13]. Experimental dynamos thus require to operate large amounts of liquid metal at very large mechanical power which explains the difficulties in observing the dynamo effect.

Finally, we note that the three flows chosen for the experimental dynamos all have domains where the helicity is strong. Helicity is a measure of how the flow breaks mirror symmetry. It is associated to a local amplification mechanism, named α effect, see [5] for a description of the relation between helicity and the α effect.

2.2. *The Ponomarenko-type dynamo in Riga*

The experiment conducted by Gailitis et al. [7] is based on one of the simplest models of homogeneous dynamo, introduced by Ponomarenko in 1973 [14]. Ponomarenko's flow involves a conductive cylinder immersed in a static infinite environment of identical conductivity, with which it is in electrical contact, performing both a uniform rotation and a translation along its axis. When the flow speed reaches a sufficiently high value, so that R_m reaches the instability threshold, this flow generates a magnetic field in the form of a helical wave. The instability is oscillatory and the helical wave propagates in the direction of the flow.

The experiment set up by the Riga group is sketched in Figure 2. The flow is generated by a propeller, creating a helical flow in a central cylindrical cavity. The return flow occurs in a ring surrounding this central flow. This flow changes the nature of the instability from convective to absolute [15]. A layer of liquid at rest is located around these two first layers. The width of the experiment is $0.8m$ and its height $3m$.

The growth of the magnetic field is observed at a driving power close to $100kW$ [15]. The nature of the bifurcation as well as the growth rates of the dynamo were found to be in good agreement with kinematic theory [7]. The measured magnetic field is about $1mT \simeq 10G$ measured at the external boundary of the layer at rest and can reach around $100mT$ at the inner cylinder where the amplification processes are the largest [16].

2.3. *The Roberts-type dynamo in Karlsruhe*

The experiment in Karlsruhe, Germany, is inspired by a kinematic dynamo model developed by G.O. Roberts [17], which showed that various periodic flows can generate a magnetic field at large scale relative to the spatial periodicity of the flow, see [18] for a recent discussion of mean-field dynamos.

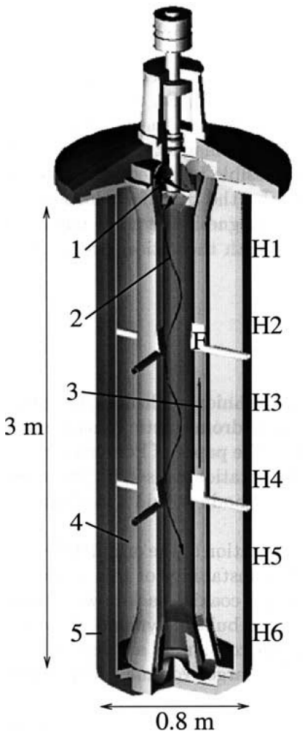

Figure 1. Sketch of Riga's experiment from [15]. A propeller (1) drives an helical flow of liquid sodium in the most inner cylindrical cavity (2). A return flow (3) is located in a second cavity and a layer of sodium at rest (4) is around these two layers. (5) is the thermal insulation. H and F indicate the positions of hall probes and of a fluxgate.

The experiment consists of 52 cells located in a cylinder with a width of $1.85m$, through which liquid sodium circulates [8]. The flow in each cell is helical, so that it generates an α-effect.

When the speed is sufficiently high, a magnetic field is generated by dynamo action. The structure of the generated field, a dipole with axis perpendicular to the z-direction, is in agreement with what is expected from a dynamo generated by the α-effect of the flow. The measured generated field is up to 350 G in the core of the experiment [19]. Estimating the power required to drive the flow from the pressure drop in the pumps that drive the flow multiplied by the flow rate, an order of magnitude slightly larger than 10 kW is obtained in the vicinity of the onset of instability. Measurements above the onset lead to an estimate of the Joules dissipation that is in agreement with a scaling law for the power dissipation derived from a set of numerical simulations. Assuming that this prediction holds for the Earth provides information on several aspects of the Earth dynamics, and in particular for the age of the inner core and for the absence of need for radioactive heating [20].

2.4. *The Von Karman Sodium dynamo*

The Von Karman Sodium (VKS) experiment is a collaboration between ENS Paris, ENS Lyon, and CEA, with the experiment being conducted at CEA-Cadarache.

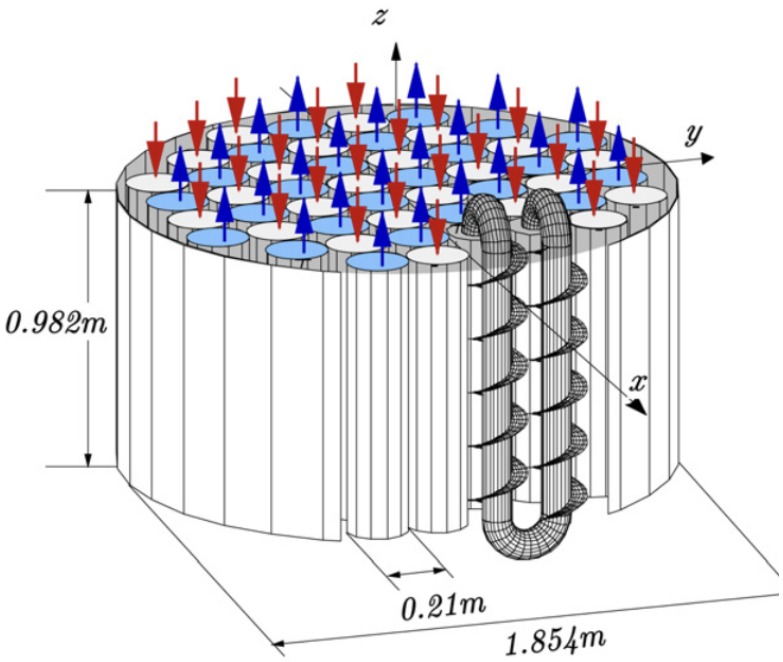

Figure 2. Sketch of Karlsruhe's experiment, figure from [19]. An array of 52 cells in which liquid sodium flows and generates an α-effect. The color arrows represent the axial direction of the flow.

The setup consists of a counter-rotating flow driven by the motion of two soft iron disks equipped with blades and located in a cylinder, see Figure 3. 150 liters of liquid sodium are set in motion by a mechanical power up to 300 kW [9].

For sufficient rotation of the disks with equal and opposite speeds, a magnetic field is observed whose large scales are dominated by an axial dipole. The dipole axis is parallel to the rotation axis of the disks. The fields fluctuates because of the turbulent fluctuations of the flow and yet the direction of the dipole remains fixed.

Unlike the two previous experiments, the time-averaged flow is not close to a known laminar flow that would generate a dynamo. Cowling's anti-dynamo theorem [5] implies that a dipolar field generated by the averaged flow should be a transverse field in order to break the azimuthal invariance of the averaged flow. Therefore, the non-axisymmetric velocity fluctuations are involved in the generation of the large-scale magnetic field.

The observations are consistent with an α-ω type mechanism, where the azimuthal shear is the source of the ω effect, while speed fluctuations due to the helical vortices near the blades are the source of the α effect [13]. Several numerical simulations have subsequently measured these effects and discussed the role of the soft iron disks [22–25]. An explanation for the role of soft iron is that it allows both the toroidal and the poloidal magnetic field component to be strong in the vicinity of the disk near the domain where the α effect is strong [26]. This lowers the instability threshold that can then be reached in the experiment. A magnetic field of amplitude up to $100-200$ G is measured in the bulk of the flow.

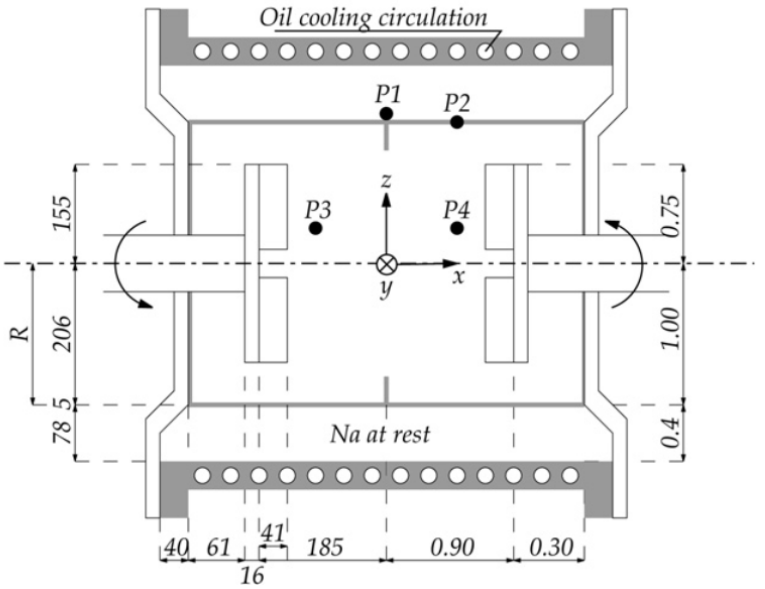

Figure 3. Sketch of VKS experiment, figure from [21]. Two soft iron discs put into motion 150 l of liquid sodium. A layer at rest is located around the swirling flow but has been removed without changing qualitatively the behavior. An oil cooling circulation maintains the temperature above the sodium melting point.

3. What the experiments taught us

3.1. *Generation mechanisms and saturation of the magnetic field*

The standard α and ω effects, enable the generation of a dynamo for flows close to laminar dynamos, but also for flows with turbulent fluctuations at all scales, as seen in the VKS experiment.

The observed magnetic field is approximately 10 to 100 G at 10% above the instability threshold. These observations are explained by the scaling law predicted for turbulent dynamos [27]. In particular, the saturation of the magnetic field results from a balance between the Laplace force and the inertial term of the Navier–Stokes equation acting on the modification of the velocity field.

A balance between the Laplace force and the viscous term of the Navier–Stokes equation can be captured analytically close to the onset of dynamo instability or numerically for a balance with the inertial term [28,29]. The order of magnitude of the generated magnetic field will not be relevant for an astrophysical object, as they are independent of the global rotation.

A similar argument can be used to take into account rotation [27], which is usually the dominant term in astrophysical objects. This leads to the order of magnitude estimate $B^2 = \frac{\rho\Omega}{\sigma}(R_m - R_{mc})$ with Ω the angular velocity. The prefactor $\sqrt{\rho\Omega/\sigma}$ is close to $10\,G$ which is not unrealistic for the Earth magnetic field. More details on the generation processes and on the saturation properties can be found in [13].

3.2. *Dynamical regimes*

An important symmetry property of the VKS experiment is that in exact counter-rotation, the forcing is symmetrical under rotation of π around any axis in the mid-plane. We denote such a

rotation by R_π. In that situation, we already mentioned that the direction of the dipolar unstable mode does not change.

When this symmetry is broken by rotating one disk faster than the other, dynamical regimes are observed such as periodic reversals as seen in the Sun, random reversals as produced by the Earth's dipole or bursting behaviors [30,31]. Examples of time series are displayed in Figure 4.

We note that a minute change of forcing parameters allows the field to transition from stationary to time periodic oscillation and to random reversals. A consequence is that the nature of the observed magnetic field is not predictive of the induction mechanism operating in the fluid. This has implications for astrophysical observations as one could be tempted to link magnetic field behavior with flow properties.

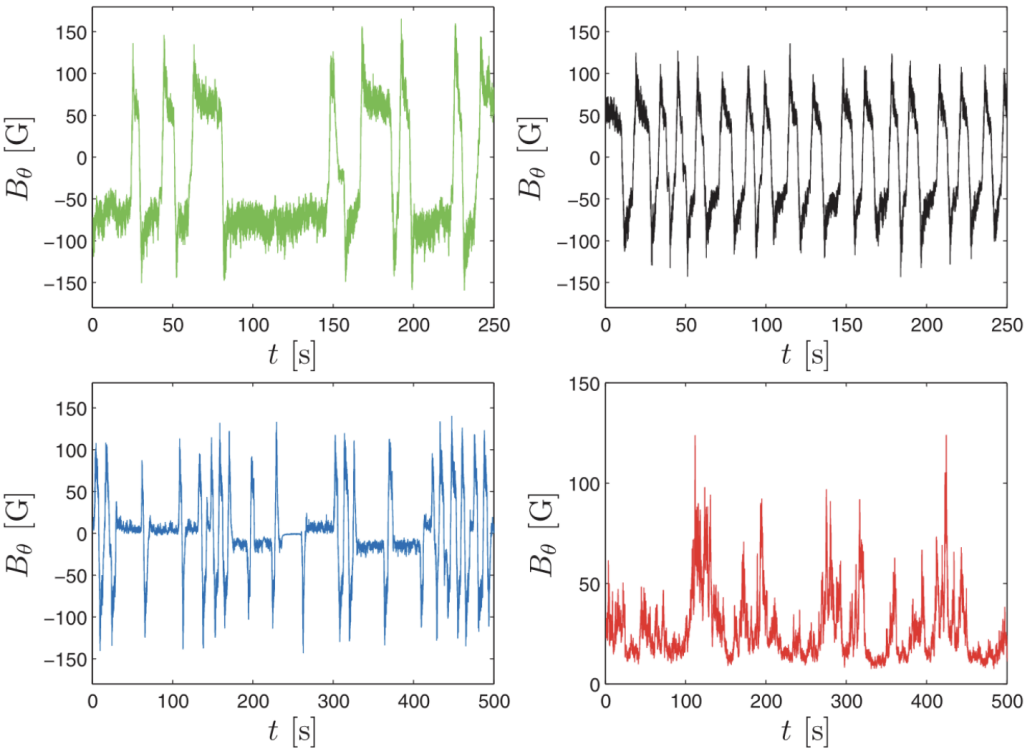

Figure 4. Time series of the azimuthal component of the magnetic field generated in the VKS experiment. One of the disks rotates faster than the other one. The different regimes are obtained by a change of temperature or a change of speed of one of the motors. These modifications result in a relative change of R_m or R_e that is smaller than 7%. See [31] for details.

The field behavior results from the competition between two modes: the dipolar mode as observed in exact counter-rotation and a second mode of quadrupolar symmetry [32]. The spatial structure of these modes is sketched in Figure 5.

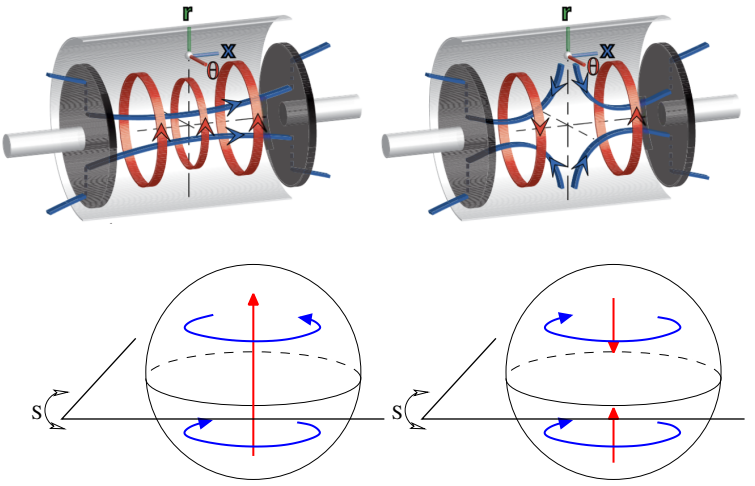

Figure 5. Schematic of the spatial structure of the large scales of the unstable modes. Left: dipolar field; right: quadrupolar field. Top: in the VKS experiment figure from [31]. Bottom: for the geodynamo. Note the different behavior of the poloidal and toroidal components of the different modes with respect to (top) the R_π symmetry around the axis noted r, (bottom) the planar reflection with respect to the equatorial plane.

4. A low-dimensional approach to the dynamics of the magnetic field

4.1. *Two competing magnetic modes*

The simplest model that describe the observations from the VKS experiment is based on the competition between two magnetic field modes [33,34]. A review and a comparison with other models is presented in [35]. The two modes involved in the dynamics have, at large scale, a dipolar structure and a quadrupolar one. The same model can be introduced to describe the dynamics of the Earth's magnetic field and the spatial structure of the modes is displayed in Figure 5 bottom. We note that these two modes transform differently with respect to the equatorial symmetry (in the case of the geodynamo) and with respect to R_π the rotation of angle π about any axis contained in the median plane (in the case of the VKS dynamo). These different symmetries notably explain the spatial structure of the toroidal field of each mode.

We assume that each mode is close to its instability threshold. We then write the total field as

$$\mathbf{B}(\mathbf{r},\mathbf{t}) = d(t)\mathbf{D}(\mathbf{r}) + q(t)\mathbf{Q}(\mathbf{r})\,, \tag{3}$$

where $\mathbf{D}(\mathbf{r})$ and $\mathbf{Q}(\mathbf{r})$ are the spatial structures as schematized in Figure 5 and $d(t)$ and $q(t)$ their amplitudes.

Let's note $A = d + iq$. Near their instability threshold, the evolution equation for A is

$$\dot{A} = \mu A + \nu \bar{A} + \mathrm{NL}(A)\,, \tag{4}$$

where $\mu = \mu_r + i\mu_i$, $\nu = \nu_r + i\nu_i$ are complex coefficient and NL(A) stands for non linear terms, of cubic order at least due to the invariance of the magnetohydrodynamic equations under change of sign of the magnetic field ($B \to -B$).

The difference in behavior of the two modes with respect to the equatorial symmetry (or the R_π rotation for VKS) implies the following property: if the flow has this symmetry, then the imaginary

parts of μ and ν are zero. The amplitude of these imaginary parts is thus a measure of how much the symmetry is broken by the flow.

It is possible to keep all the nonlinear term of cubic order [33] but for simplicity we assume that they will simply maintain fix the norm of A. In other words, we note $A = r \exp i\theta$ and assume that the effect of the nonlinear term in Eq. (4) is to enforce r to remain at a constant value. Then θ can be shown to satisfy

$$\dot{\theta} = \mu_i + \nu_i \cos(2\theta) - \nu_r \sin(2\theta) . \tag{5}$$

4.2. *Random or periodic reversals*

Let's first discuss the case where μ_i is significantly larger than ν_i and thus set $\nu_i = 0$. For small μ_i, Eq. (5) has 4 steady solutions, 2 of which are stable and 2 are unstable, see Figure 6. Note that the phase space remains invariant under central symmetry through the origin, as a consequence of the $B \to -B$ invariance of the MHD equations.

A weak breaking of the symmetry brings the stable fixed points closer to the unstable fixed points in the phase space but the solution remains stationary. When $\mu_i > \nu_r$, there is no longer any stationary solution, and the solution becomes a non-linear oscillation. In other words, at $\mu_i = \nu_r$ a saddle-node bifurcation transforms the pair of stable solutions into a limit cycle: the magnetic field becomes oscillatory. Its spatial structure evolves over time from a dipole to a quadrupole to the opposite of the initial dipole, the opposite of the initial quadrupole and back to the initial dipole.

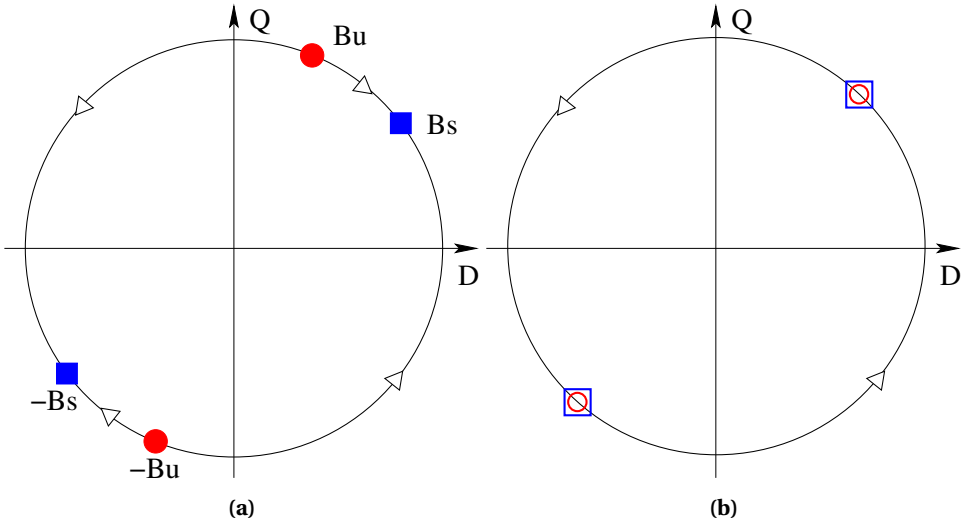

Figure 6. Phase space close to the saddle node bifurcation. Left: the two stable state B_s are at finite distance of the unstable ones B_u. Right: At the onset of the saddle node bifurcation, the steady states collide and disappear and a limit cycle appears. Figures from [34].

In addition to this periodic oscillation behavior, this system can easily generate random reversals. We assume that we are close to the threshold of the bifurcations as in Figure 6(a) and we model the effect of turbulent fluctuations by random perturbations that cause the system state to diffuse in the phase space.

If the solution is initially located close to one of the stable fixed points, say B_s, fluctuations can push the system away from B_s. If it goes beyond the unstable fixed point B_u, it is attracted by the

opposite fixed point $-B_s$, and thus achieves a polarity reversal. Several properties arise from this mechanism:

- A reversal is made of two successive phases. The first phase $B_s \to B_u$ in Figure 6(a) is the approach toward an unstable fixed point. The deterministic dynamics acts against the evolution, and this phase is slow. The second phase $B_u \to -B_s$, is fast since the deterministic dynamics favors the motion.
- At the end of the first phase, the system may return toward the initial stable fixed point (phase $B_u \to B_s$), which corresponds to an aborted reversal or an excursion. Notably, the Earth dipole has displayed several excursions in the past.
- At the end of a reversal, the dipolar amplitude $d(t)$ reaches large values before it tends towards the value of the dipolar part of B_s: this is an overshoot. In contrast, excursions do not display overshoots.

These prediction can be easily tested on Eq. (4) by adding a stochastic term that models the effect of the turbulent fluctuations. Time series are displayed in Figure 7. We also display time series of the Earth dipole and of the magnetic field measured in the VKS experiment. The aforementioned properties are clearly displayed by the three systems: existence of reversals and of excursions, the existence of a slow and a fast phase during the reversal, the overshoot at the end of the reversal and its absence for the excursions.

4.3. *Hemispherical dynamos*

The model of competition between dipole and quadrupole also allows for the description of another regime of interest: when the symmetry is broken but the dominant term in Eq. (5) is ν_i. Then the solution remains stationary and corresponds to $\theta = \pi/4, 5\pi/4$. This means that the dipole and quadrupole are of equal amplitudes as $d = r\cos\theta$ and $q = r\sin\theta$. On one side of the Earth's core or the VKS dynamo, the two modes add together, while on the other side, they subtract. Thus, we are in the presence of a hemispherical or localized dynamo [37]. This regime could possibly be that of Mars' field in the past and has also been observed in the VKS experiment [38].

It is quite remarkable that the same mechanism of competition between a dipolar mode and a quadrupolar mode allows for capturing such diverse regimes as random or periodic reversals, burst behaviors, or hemispheric modes.

4.4. *Role of symmetry breaking*

When the dynamics involve a dipolar mode and a quadrupolar mode, it is the breaking of symmetry that couples the two modes and allows for reversals of the field or for localized dynamos.

In the case where reversals are generated by the coupling, it can be shown that the frequency of the reversals increases with the amplitude of the symmetry breaking [34].

This breaking of symmetry is controlled in the VKS experiment by the difference in rotation between the two discs. On Earth, several origins of symmetry breaking can be thought of: spontaneous fluctuations in the large-scale structure of the flow in the liquid core, asymmetric forcings at the core-mantle boundary, or similar effects at the level of the solid core. In the following section, using what we have understood about the mechanism of magnetic field reversal, we will propose an explanation for the long-term variability in the frequency of the geodynamo reversals. It relies on the mantle dynamics and thus relates plate tectonics to the dynamo of the liquid core.

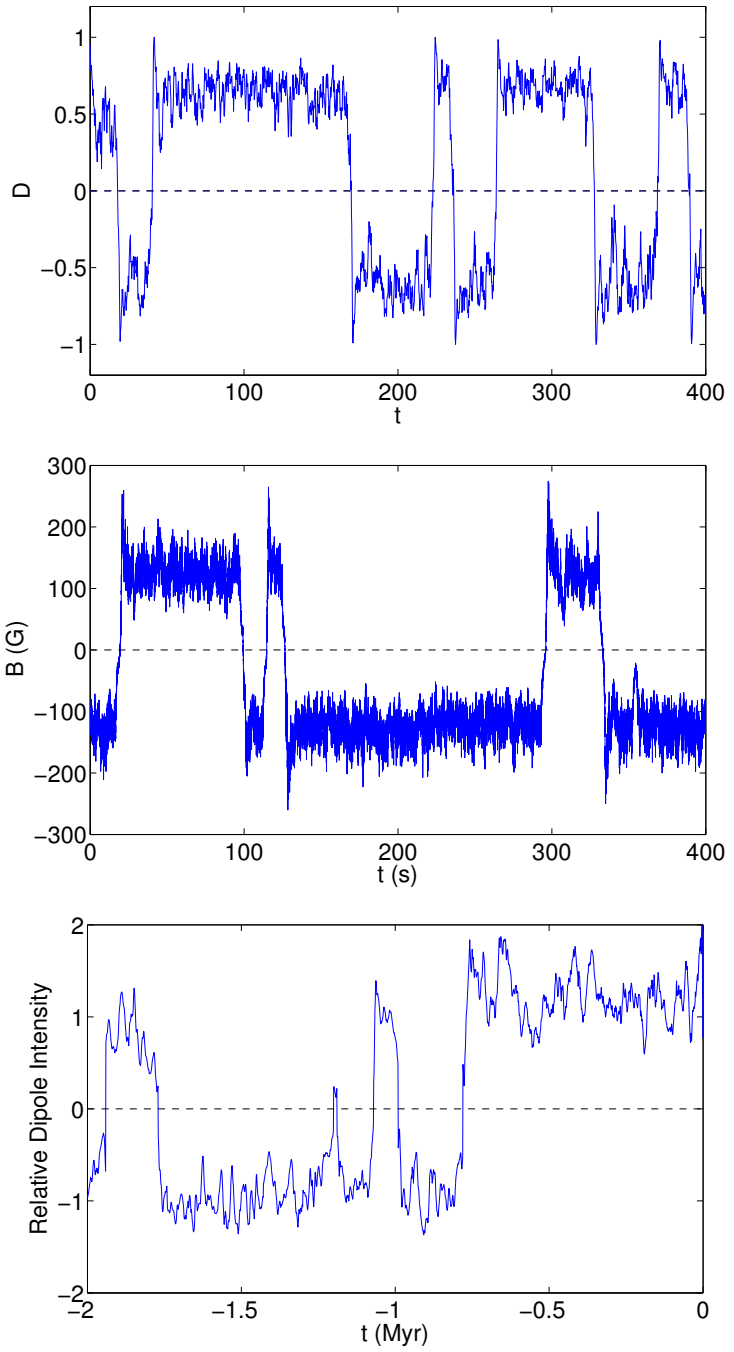

Figure 7. (Top) Time series of the dipole amplitude for a system below the threshold of the saddle-node bifurcation (Eq. (5)) subject to noise. (Middle) Time series of the magnetic field measured in the VKS experiment for the two impellers rotating with different frequencies in the regime of random reversals (data from [30]). (Bottom) Composite paleointensity curve for the past 2 millions years (data from [36]).

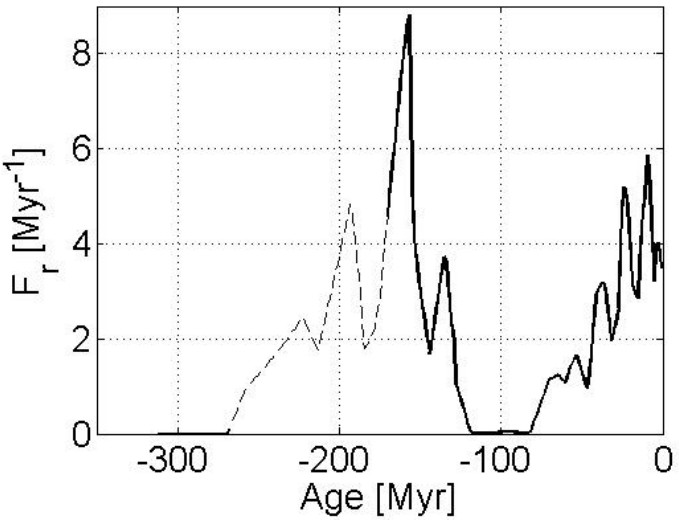

Figure 8. Reversal frequency as a function of age, data from [41].

5. Plate Tectonics and the Frequency of Reversals

The number of reversals of the Earth's magnetic field per unit of time has not remained constant over time. Over the last 80 million years, the average frequency, see Figure 8, has increased from zero reversals during the Cretaceous Normal Superchron (CNS) between 80 and 120 million years ago to about 4 per million years over the last 5 million years (Myr). Before this superchron, the frequency decreased over several tens of millions of years. We also note that older superchrons have been measured. Therefore, the frequency of reversals follows long-term variations over durations of several tens of millions of years, see discussions in [39] or [40].

Among the physical phenomena that determine the evolution of the Earth, few are associated with such a time scale. Ultimately, it is the convective movements in the mantle, and thus plate tectonics, that seems to be the most capable of explaining the variability in the frequency of reversals. Indeed, the characteristic time scale built upon the typical velocity of plates say 10cm/yr over the Earth radius 6000km is 60Myr and is of the correct order of magnitude.

Considering what we have learned from modeling the reversals of the magnetic field, as described in Section 4, a coupling between plate tectonics and properties of the dynamo in the liquid core is possible provided there exists a breaking of equatorial symmetry of the boundary conditions at the core mantle boundary (CMB).

Assuming that the properties at the CMB are correlated with the ones at the surface of the mantle, we have studied the arrangement of continents, which has been known for over 300 million years, as seen in Figure 9. We note that their arrangement in relation to the equator varies and alternates between globally symmetrical arrangements and arrangements preferentially in one hemisphere. In particular, the recent evolution between age 65 Myr and present time (figure b and a) and the one between age 260 and 200 Myr (figure d and c) are associated to a drift of the continent position away from an equatorially symmetric position towards a more northern one. During these periods, the reversal frequency increases.

To quantify this effect, we have determined the convex hull of the continents and then calculated $D = \int z dS/St$ where z is the distance to the equator, the sum is taken over the convex hull, and St is the total surface area of the Earth. This term thus measures how asymmetrical the distribution of continents is in relation to the equator.

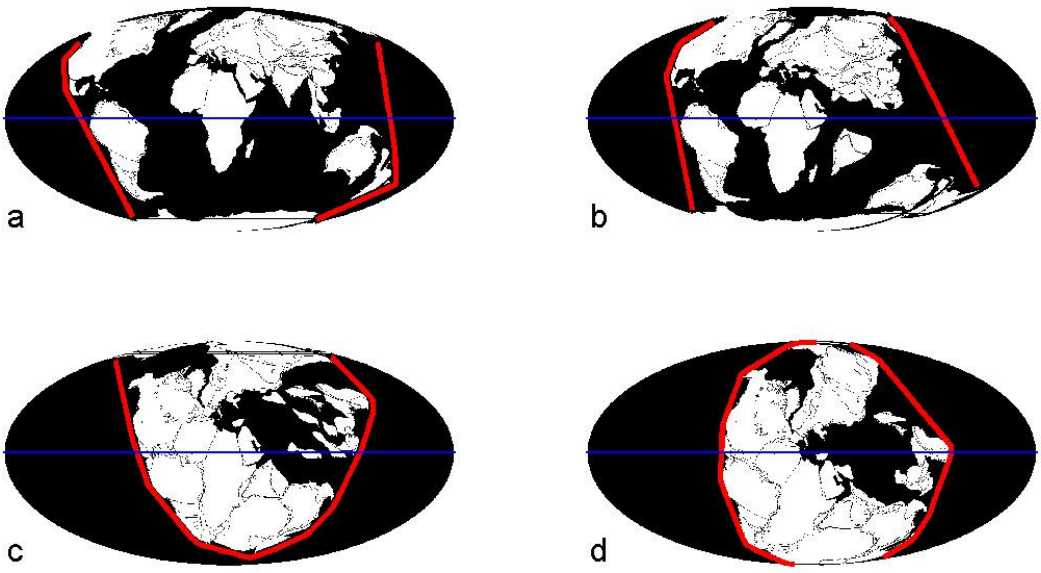

Figure 9. Position of the continents with their convex envelope (red line) at various periods of time: (a) present time, (b) 65 Myr ago, (c) 200 Myr ago, (d) 260 Myr ago. Figure from [39].

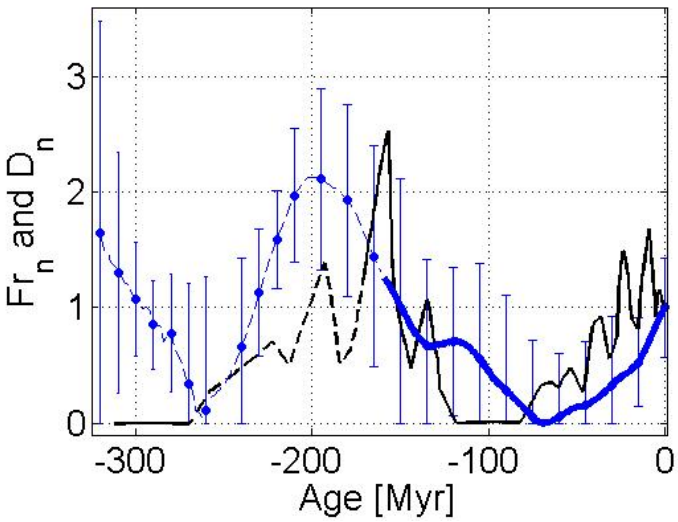

Figure 10. Comparison between changes in reversal frequency (black line) and the D parameter obtained after $D_n = |D - D(-65Myr)|$ (blue line). The bold line corresponds to the past 170 Ma documented by magnetic oceanic anomalies. Error bars represent uncertainties in continental reconstructions. Both curves have been normalized to their present value. Figure from [39].

The characteristic time of variation of D is similar to that of the frequency of reversals and we observe that D presents a minimum 65 million years ago. If we plot the deviation $|D-D(65Myr)|$ as a function of time, the curve is similar to that of F_r, see Figure 10.

We deduce that the position of the continents is correlated with the frequency of reversals and, based on our understanding of the origin of variability of the reversal frequency, this is coherent with a control of the reversal frequency by plate tectonics.

Let us now discuss a possible mechanisms at work. We know that it is the equatorial symmetry of the flow in the liquid core that is important and that this is therefore correlated with the position of the continents. The most direct explanation is as follows: the continents affect the large-scale temperature structure in the mantle, especially since they determine the areas where cold matter descends and where hot plumes rise. This has been verified numerically [42] who observe that supercontinents promote temperature anomalies on the largest scales. These spatial variations in temperature and composition propagate to the CMB (core-mantle boundary) where they affect the equatorial symmetry of the flow. This modifies the reversal frequency as explained in Section 4.

6. Conclusions

Dynamo experiments have notably demonstrated the validity of amplification mechanisms, their ability to generate a magnetic field at large scale, and their robustness for very turbulent flows.

Random or periodic reversals of the magnetic field as seen in astrophysical objects are generic behaviors. They result from the competition between a small number of modes, and a dynamical system approach allows us to identify their origin and to predict other behaviors, such as hemispherical dynamos, which have also been observed.

For the geodynamo, it is the equatorial symmetry of the flow that plays a role in the case of competition between a dipole and a quadrupole. In particular, this symmetry breaking determines the frequency of reversals. We have shown that variations of the reversal frequency on time scales of 100 million years are correlated with the position of the continents. This indicates a strong coupling between what is observed on the surface of the mantle and what happens at the core-mantle boundary and then in the liquid core.

To finish, we mention some related problems of interest.

Geodynamo simulations. Numerical simulations of the geodynamo do not clearly observe a dipole-quadrupole coupling, except for some specific parameter values such as [43] or [44]. Numerical simulations are bound to run with P_m not too small. P_m of order unity implies that the velocity modes and the magnetic ones have similar dissipative time scale. This is quite different from the realistic situation of a liquid metal for which $P_m < 10^{-5}$ so that the magnetic modes are heavily damped compared to the velocity ones. We expect that decreasing P_m in numerical simulations will simplify the dynamics of the magnetic field that will be less sensitive to the velocity turbulent fluctuations.

Low dimensional chaos. The coupling of two magnetic modes with a single hydrodynamic degree of freedom is sufficient to generate chaotic attractors for which the dipolar amplitude changes sign [45]. This regime might be observable in numerical simulations with order one P_m and at moderate forcing so that a small number of hydrodynamic and magnetic modes are dynamically coupled and evolve at similar timescales.

Properties of mantle convection. Numerical models of the mantle can be used to investigate further the relation between the surface (location of the continents, of the descending and ascending material, etc…) and the boudary condition enforced to the liquid core at the CMB, see for instance [46].

Earth magnetic field measurements. Some measurements of the magnetic field in the last 100 thousand years have a temporal resolution that could be precise enough to estimate the quadrupolar component of the magnetic field. It would be interesting to investigate its behavior, for instance during the more recent excursions.

Precession driven dynamos. Efforts are currently ongoing in the development of an experimental dynamo based on a precession driven flow, see the related article in this article collection. This forcing mimicks the effect of the precession of the rotating axis of astrophysical objects when tides are the dominant forcing. If a magnetic field is generated by the dynamo instability, it will be interesting to investigate whether dynamical regimes appear as a result from the competition between a small number of unstable modes.

Acknowledgments

I thank Stephan Fauve for many discussions and suggestions that drove our researches on this topic. I also thank Basile Gallet, Christophe Gissinger with whom I collaborated on part of the works reviewed in this article and also all the other members of the VKS collaborations with whom the data obtained in [9,21,30,31] were obtained. I also acknowledge Emmanuel Dormy, Jean-Pierre Valet and Jean Besse for discussions and collaborations on the geodynamo and on plate tectonics. I thank F. Stefani and the authors of [15] and A. Tilgner and the authors of [19] for providing figures or datas from their publications.

Declaration of interests

The authors do not work for, advise, own shares in, or receive funds from any organization that could benefit from this article, and have declared no affiliations other than their research organizations.

References

[1] J. Larmor, "How could a rotating body such as the sun become a magnet?", in *Rep. 87th Meeting Brit. Assoc. Adv. Sci., Bornemouth, Sept. 9–13*, John Murray: London, 1919, pp. 156–160.

[2] F. Lowes and I. Wilkinson, "Geomagnetic Dynamo: An Improved Laboratory Model", *Nature* **219** (1968), pp. 717–718.

[3] A. A.-Z. Raúl and P. Jānis, "Realization of Bullard's disc dynamo", *Proc. R. Soc. Lond., Ser. A* **479** (2023), article no. 20220740.

[4] F. Alboussière T. Plunian and M. Moulin, "Fury: an experimental dynamo with anisotropic electrical conductivity", *Proc. R. Soc. Lond., Ser. A* **478** (2022), article no. 20220374.

[5] H. K. Moffatt, *Magnetic Field Generation in Electrically Conducting Fluids*, Cambridge Monographs on Mechanics and Applied Mathematics, Cambridge University Press: Cambridge, 1978.

[6] Y. B. Zeldovich, A. A. Ruzmaikin and D. D. Sokoloff, *Magnetic Fields in Astrophysics*, The Fluid Mechanics of Astrophysics and Geophysics, Gordon and Breach Science Publishers: New York, 1983.

[7] A. Gailitis, O. Lielausis, E. Platacis, et al., "Magnetic field saturation in the Riga dynamo experiment", *Phys. Rev. Lett.* **86** (2001), pp. 3024–3027.

[8] R. Stieglitz and U. Müller, "Experimental demonstration of a homogeneous two-scale dynamo", *Phys. Fluids* **13** (2001), pp. 561–564.

[9] R. Monchaux, M. Berhanu, M. Bourgoin, et al., "Generation of magnetic field by dynamo action in a turbulent flow of liquid sodium", *Phys. Rev. Lett.* **98** (2007), article no. 044502.

[10] N. L. Peffley, A. B. Cawthorne and D. P. Lathrop, "Toward a self-generating magnetic dynamo: The role of turbulence", *Phys. Rev. E* **61** (2000), no. 5, pp. 5287–5294.

[11] M. D. Nornberg, E. J. Spence, R. D. Kendrick, C. M. Jacobson and C. B. Forest, "Measurements of the magnetic field induced by a turbulent flow of liquid metal", *Phys. Plasmas* **13** (2006), no. 5, article no. 055901.

[12] S. Cabanes, N. Schaeffer and H.-C. Nataf, "Magnetic induction and diffusion mechanisms in a liquid sodium spherical Couette experiment", *Phys. Rev. E* **90** (2014), article no. 043018.

[13] F. Pétrélis, N. Mordant and S. Fauve, "On the magnetic fields generated by experimental dynamos", *Geophys. Astrophys. Fluid Dyn.* **101** (2007), no. 3-4, pp. 289–323.
[14] Y. B. Ponomarenko, "Theory of the hydromagnetic generator", *J. Appl. Mech. Tech. Phys.* **14** (1973), pp. 775–778.
[15] A. Gailitis, O. Lielausis, E. Platacis, G. Gerbeth and F. Stefani, "The Riga Dynamo Experiment", *Surv. Geophys.* **24** (2003), pp. 247–267.
[16] A. Gailitis, G. Gerbeth, T. Gundrum, O. Lielausis, G. Lipsbergs, E. Platacis and F. Stefani, "Self-excitation in a helical liquid metal flow: the Riga dynamo experiments", *J. Plasma Phys.* **84** (2018), no. 3, article no. 735840301.
[17] G. O. Roberts, "Dynamo action of fluid motions with two- dimensional periodicity", *Philos. Trans. R. Soc. Lond., Ser. A* **271** (1972), pp. 411–454.
[18] A. Alexakis, S. Fauve, C. Gissinger and F. Pétrélis, "Effect of fluctuations on mean-field dynamos", *J. Plasma Phys.* **84** (2018), no. 4, article no. 735840401.
[19] U. Müller, R. Stieglitz, F. H. Busse and A. Tilgner, "The Karlsruhe two-scale dynamo experiment", *Comptes Rendus. Physique* **9** (2008), no. 7, pp. 729–740.
[20] U. Christensen and A. Tilgner, "Power requirement of the geodynamo from ohmic losses in numerical and laboratory dynamos", *Nature* **429** (2004), pp. 169–171.
[21] S. Aumaître, M. Berhanu, M. Bourgoin, et al., "The VKS experiment: turbulent dynamical dynamos", *Comptes Rendus. Physique* **9** (2008), no. 7, pp. 689–701.
[22] C. J. P. Gissinger, "A numerical model of the VKS experiment", *Eur. Phys. Lett.* **87** (2009), no. 3, article no. 39002.
[23] A. Giesecke, F. Stefani and G. Gerbeth, "Role of Soft-Iron Impellers on the Mode Selection in the von Kármán–Sodium Dynamo Experiment", *Phys. Rev. Lett.* **104** (2010), no. 4, article no. 044503.
[24] C. Nore, J. Léorat, J.-L. Guermond and A. Giesecke, "Mean-field model of the von Kármán sodium dynamo experiment using soft iron impellers", *Phys. Rev. E* **91** (2015), no. 1, article no. 013008.
[25] S. Kreuzahler, Y. Ponty, N. Plihon, H. Homann and R. Grauer, "Dynamo Enhancement and Mode Selection Triggered by High Magnetic Permeability", *Phys. Rev. Lett.* **119** (2017), no. 23, article no. 234501.
[26] J. Herault and F. Pétrélis, "Optimum reduction of the dynamo threshold by a ferromagnetic layer located in the flow", *Phys. Rev. E* **90** (2014), article no. 033015.
[27] F. Pétrélis and S. Fauve, "Saturation of the magnetic field above the dynamo threshold", *Eur. Phys. J. B, Condens. Matter Complex Syst.* **22** (2001), pp. 273–276.
[28] A. Tilgner and F. H. Busse, "Simulation of the bifurcation diagram of the Karlsruhe dynamo", *Magnetohydrodynamics* **38** (2002), pp. 35–40.
[29] A. Nunez, F. Petrelis and S. Fauve, "Saturation of a Ponomarenko type fluid dynamo", in *Dynamo and Dynamics, a Mathematical Challenge* (P. Chossat, D. Armbruster and I. Oprea, eds.), NATO Science Series, Kluwer Academic Publishers : Dordrecht, 2001, pp. 67–74.
[30] M. Berhanu, R. Monchaux, S. Fauve, et al., "Magnetic field reversals in an experimental turbulent dynamo", *Eur. Phys. Lett.* **77** (2007), no. 5, article no. 59001.
[31] F. Ravelet, M. Berhanu, R. Monchaux, et al., "Chaotic Dynamos Generated by a Turbulent Flow of Liquid Sodium", *Phys. Rev. Lett.* **101** (2008), no. 7, article no. 074502.
[32] C. Gissinger, "Dipole-quadrupole dynamics during magnetic field reversals", *Phys. Rev. E* **82** (2010), no. 5, article no. 056302.
[33] F. Pétrélis and S. Fauve, "Chaotic dynamics of the magnetic field generated by dynamo action in a turbulent flow", *J. Phys. Cond. Matt.* **20** (2008), no. 49, article no. 494203.
[34] F. Pétrélis, S. Fauve, E. Dormy and J.-P. Valet, "Simple Mechanism for Reversals of Earth's Magnetic Field", *Phys. Rev. Lett.* **102** (2009), article no. 144503.
[35] F. Pétrélis and S. Fauve, "Mechanisms for magnetic field reversals", *Philos. Trans. R. Soc. Lond., Ser. A* **368** (2010), no. 1916, pp. 1595–1605.
[36] J.-P. Valet, L. Meynadier and Y. Guyodo, "Geomagnetic dipole strength and reversal rate over the past two million years", *Nature* **435** (2005), pp. 802–805.
[37] B. Gallet and F. Pétrélis, "From reversing to hemispherical dynamos", *Phys. Rev. E* **80** (2009), no. 3, article no. 035302.
[38] B. Gallet, S. Aumaître, J. Boisson, et al., "Experimental Observation of Spatially Localized Dynamo Magnetic Fields", *Phys. Rev. Lett.* **108** (2012), no. 14, article no. 144501.
[39] F. Pétrélis, J. Besse and J.-P. Valet, "Plate tectonics may control geomagnetic reversal frequency", *Geophys. Res. Lett.* **38** (2011), no. 19, article no. L19303.
[40] V. Courtillot and P. Olson, "Mantle plumes link magnetic superchrons to phanerozoic mass depletion events", *Earth Planet. Sci. Lett.* **260** (2007), no. 3, pp. 495–504.
[41] S. C. Cande and D. V. Kent, "Revised calibration of the geomagnetic polarity timescale for the Late Cretaceous and Cenozoic", *J. Geophys. Res. Solid Earth* **100** (1995), no. B4, pp. 6093–6095.
[42] B. R. Phillips and H.-P. Bunge, "Heterogeneity and time dependence in 3D spherical mantle convection models with continental drift", *Earth Planet. Sci. Lett.* **233** (2005), no. 1, pp. 121–135.

[43] J. Li, T. Sato and A. Kageyama, "Repeated and Sudden Reversals of the Dipole Field Generated by a Spherical Dynamo Action", *Science* **295** (2002), no. 5561, pp. 1887–1890.

[44] J. Wicht and P. Olson, "A detailed study of the polarity reversal mechanism in a numerical dynamo model", *Geochemistry, Geophys. Geosystems* **5** (2004), no. 3, article no. Q03H10.

[45] C. Gissinger, "A new deterministic model for chaotic reversals", *Eur. Phys. J. B, Condens. Matter Complex Syst.* **85** (2012), article no. 137.

[46] T. Frasson, S. Labrosse, H.-C. Nataf, N. Coltice and N. Flament, "On the impact of true polar wander on heat flux patterns at the core-mantle boundary", *EGUsphere* **2023** (2023), pp. 1–24.